# Stochastic subgrid model with scaling laws for oceanic simulations

**V. Kitsios[1], J. S. Frederiksen[1] and M. J. Zidikheri[2]**

[1]Centre for Australian Weather and Climate Research (CAWCR),
CSIRO Marine and Atmospheric Research, Aspendale 3195, AUSTRALIA

[2]CAWCR, Australian Bureau of Meteorology, Melbourne 3001, AUSTRALIA

## Abstract

Stochastic and deterministic subgrid-scale parameterisations are developed for the large eddy simulation (LES) of oceanic flows. Parameterisations are developed for a flow representative of the Antarctic Circumpolar Current (ACC), generated using a spectral quasi-geostrophic code. The subgrid eddy viscosity coefficients are calculated using the approach of [3], whereby a high resolution reference direct numerical simulation (DNS) is truncated back to the LES truncation wavenumber $T_R$. Two subgrid parameterisations are produced: isotropic, in which the coefficients are only dependent on the total wavenumber ($n$); and anisotropic, in which the coefficients are also dependent on zonal wavenumbers ($m$). These LES variants reproduce the kinetic energy spectra of the DNS at various resolutions. Scaling laws are determined representing the isotropic profiles, which make the parameterisations more generally applicable, as they remove the need for a higher resolution reference simulation.

## Introduction

In geophysical flows it is not possible to resolve all of the scales of motion. Instead one must resort to LES, where the large eddies are resolved by a computational grid, and the unresolved subgrid interactions are parameterised. In three-dimensional turbulence the empirical subgrid model of [9] is typically adopted, where the contribution of the subgrid scales to the evolution of the resolved field is parameterised by an eddy viscosity. Here the eddy viscosity is given by a specified constant multiplied by a measure of the local grid size and the resolved strain rate. In simulations of two-dimensional and quasi-geostrophic (QG) turbulence, is it more appropriate for the eddy viscosity to be steeper in spectral space, taking the form of the Laplacian raised to a certain specified power. Regardless of the method, if the subgrid interactions are not parameterised properly, an increase in resolution will not necessarily increase the accuracy of the explicitly resolved scales, as illustrated in [7]. This dependence of the resolved planetary and synoptic scales on resolution has been an issue in general circulation models since the earliest geophysical simulations, and persists today in even the most sophisticated codes.

This resolution dependence problem was addressed in [2], by using renormalisation closure theory to develop stochastic subgrid parameterisations for QG turbulence. The parameterisations consist of a drain eddy viscosity and stochastic backscatter, and produced resolution independent LES. Broadening the applicability of the method to more complex flows, [3] developed a means of determining the subgrid parameterisation coefficients from the statistics of a higher resolution reference DNS coarsened to the desired LES resolution. Note the term DNS in the present context is taken to mean a high resolution reference simulation, not one that necessarily explicitly resolves all scales of motion. This approach was successfully applied to QG simulations of the atmosphere and ocean, comprising of sheared jets, Rossby waves, and baroclinic instability in [10, 11]. It was then shown in [5] that within certain regimes of the atmosphere, scal-

ing laws exist that govern how the parameterisation coefficients change with resolution. These scaling laws enable the parameterisations to be more generally applicable and remove the need to generate the subgrid coefficients from a DNS. The aim of the present paper is to produce such scaling laws for oceanic flows.

The paper is organised as follows. Firstly we summarise the QG potential vorticity equation (QGPVE), and present the resulting DNS flow fields and spectra. The LES version of the QGPVE is then outlined, along with the details on how the subgrid coefficients are determined from the DNS. The subgrid coefficients are then illustrated. A comparison is then made between the kinetic energy spectra from the DNS and various LES.

## Quasi-geostrophic DNS spectral equations

We employ the two-level QG model of [1], which captures the essential dynamics of baroclinic and barotropic instabilities. The vorticity is represented at two vertical levels, with $j = 1$ representing a depth of approximately 200m, and $j = 2$ a depth of 600m. The system is non-dimensionalised by using the radius of the Earth ($a = 6371$km) as a length scale, and the inverse of the Earth's angular velocity ($\Omega = 7.292 \times 10^{-5}$s$^{-1}$) as a time scale. By default all variables are assumed to be non-dimensional unless units are specified.

The QGPVE is spectrally discretised by expanding the field variables in spherical harmonics with the zonal (longitudinal) wavenumber $m$, and the total wavenumber $n$. This results in the prognostic equations for the spectral coefficients of the potential vorticity, $q_{mn}^j = \zeta_{mn}^j + (-1)^j F_L[\psi_{mn}^1 - \psi_{mn}^2]$ where the superscript $j$ on the flow variables denotes the level, $\zeta_{mn}^j = -n(n+1)\psi_{mn}^j$ are the spectral coefficients of the vorticity, $\psi_{mn}^j$ the streamfunction coefficients, and $n(n+1)$ is the discrete form of the Laplacian. Here $F_L$ is a layer coupling parameter, related to the Rossby radius of deformation by $r_R = 1/\sqrt{2F_L}$. The evolution equation for $q_{mn}^j$ is given by

$$\frac{\partial q_{mn}^j}{\partial t} = i\sum_{pq}\sum_{rs} K_{nqs}^{mpr} \psi_{-pq}^j q_{-rs}^j - i\omega_{mn}\zeta_{mn}^j - \alpha^j(n)\zeta_{mn}^j$$
$$+ \kappa_n(\tilde{q}_{mn}^j - q_{mn}^j) - n(n+1)\sum_{l=1}^{2} \nu_0^{jl}(m,n)q_{mn}^l , \quad (1)$$

where the summations immediately after the equals sign are over the triangular wavenumber set $\mathbf{T} = \mathbf{C}(T)$, with $T$ the DNS truncation wavenumber, and

$$\mathbf{C}(T) = [\, p,q,r,s \,|-T \leq p \leq T \,, |p| \leq q \leq T \,,$$
$$-T \leq r \leq T \,, |r| \leq s \leq T \,] . \quad (2)$$

The Rossby wave frequency is $\omega_{mn} = -Bm/[n(n+1)]$, where $B = 2$ with the chosen non-dimensionalisation. The drag at each level is $\alpha^j(n) = \alpha_{max}^j[1 - \mathrm{erf}(0.1(n-50))]/2$, where erf is the error function, and the damping times ($1/\alpha_{max}^j$) are 40 days for level 1 and 10 days for level 2. The interaction coefficients $K_{nqs}^{mpr}$
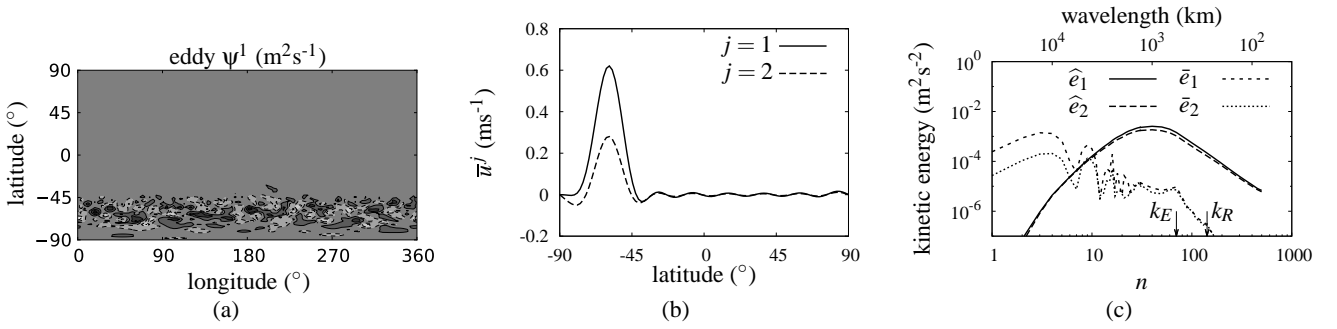
Figure 1: DNS flow field: (a) Level 1 instantaneous eddy (non-zonal) streamfunction field ($\psi^1$), with contours black$=-1.4\times10^{-6}\mathrm{m}^2\mathrm{s}^{-1}$ and white$=1.4\times10^{-6}\mathrm{m}^2\mathrm{s}^{-1}$; (b) time averaged zonal current ($\overline{u}^j$); and (c) mean ($\overline{e}_j$) and fluctuating ($\hat{e}_j$) kinetic energy spectra.

are detailed in [3]. All simulations are driven toward a mean state $\tilde{q}_{mn}^j$, that is purely zonal ($\tilde{q}_{mn}^j$ are zero unless $m=0$) and corresponds to a large-scale easterly current in the mid-latitudes of the southern hemisphere, mimicking the ACC. The simulations are driven toward this state by a relaxation parameter $\kappa_n$, which for $m=0$ and $n\leq 15$ has a relaxation time $(1/\kappa_n)$ of 11.6 days, and $\kappa_n=0$ for all remaining wavenumber pairs. The bare eddy viscosity $\nu_0^{jl}(m,n)$, is necessary as the DNS does not resolve all of the scales of motion. We represent $\nu_0^{jl}(m,n)$ in its general anisotropic matrix form (dependent on $m$ and $n$) but in our simulations it is isotropic (dependent only on $n$) where $\nu_0^{jl}(m,n)=\nu_0^{jl}(n)=\delta_{lj}\,\nu_0^{jj}(T)\,[n/T]^{\rho_0^j-2}$, and $\delta_{lj}$ is the Kronecker delta function, ensuring the off-diagonal elements are zero. Here $\nu_0^{jj}(T)$ is the value of the diagonal elements at truncation and the exponent $\rho_0^j$ determines the steepness of $\nu_0^{jj}(n)$.

**DNS flow fields and spectra**

DNS of a QG ocean is undertaken with $F_L=2.5\times10^{-10}\mathrm{m}^{-2}$, corresponding to a Rossby radius of $r_R=1/\sqrt{2F_L}=45\mathrm{km}$. The nondimensional Rossby wavenumber is $k_R=a/r_R=142$, which is consistent with the simulations of [11]. The following DNS has truncation wavenumber of $T=504$, which is equivalent to $1536\times768$ grid points (in longitude $\times$ latitude), or a grid point every 0.234 degrees. The time step size used is $\Delta t=600\mathrm{s}$, and the statistics are accumulated over a period of 6 years. Recall DNS in this context refers to a high resolution reference simulation, not one that necessarily explicitly resolves all scales of motion. Strictly speaking what is referred to as a DNS in the present paper is a high resolution reference LES.

A snapshot of the level 1 instantaneous streamfunction field ($\psi^1$) minus the zonal component is shown in Fig. 1(a), which illustrates that the dominant structures are located in the mid to high latitudes of the southern hemisphere, consistent with the ACC. The corresponding time averaged zonal current ($\overline{u}^j$) is shown as a function of latitude in Fig. 1(b). The maximum velocity of the current depths of 200m and 600m, are $\approx 0.6\mathrm{ms}^{-1}$ and $\approx 0.3\mathrm{ms}^{-1}$ respectively; consistent with measurements of the ACC [8].

The kinetic energy spectra ($e_j$) is decomposed into mean ($\overline{e}_j$) and transient ($\hat{e}_j$) energies. Figure 1(c) illustrates that the level 1 energy is greater than level 2 at all wavenumbers. The energy containing scales wavenumber $k_E\approx70$ is defined as the wavenumber at which self similar inertial range begins, and is labelled on the $n$ axis of 1(c) along with the Rossby wavenumber $k_R$. The enstrophy flux ($\eta_j$) is the rate at which enstrophy (vorticity squared) is transferred from one wavenumber to the next. On each level $j$ within the inertial range $\eta_j$ is constant, with $\eta_1=1.88\times10^{-16}\mathrm{s}^{-3}$ and $\eta_2=1.36\times10^{-16}\mathrm{s}^{-3}$. The eddy

viscosity on level $j$ is proportional to $\eta_j^{1/3}$ [6].

**Stochastic modelling of subgrid scales**

The stochastic modelling approach of [3] is used to parameterise the subgrid interactions. The resolution of a LES is lower than the associated DNS, and confined to the resolved scale wavenumber set $\mathbf{R}=\mathbf{C}(T_R)$, where $T_R$ is the LES truncation wavenumber such that $T_R<T$. The subgrid wavenumber set is defined as $\mathbf{S}=\mathbf{T}-\mathbf{R}$. To facilitate a discussion on the flow decomposition, we let $\mathbf{q}=(q_{mn}^1,q_{mn}^2)^T$ for a given wavenumber pair. In this vector notation $\mathbf{q}_t(t)=\mathbf{q}_t^{\mathbf{R}}(t)+\mathbf{q}_t^{\mathbf{S}}(t)$, where $\mathbf{q}_t$ is the tendency (time derivative) of $\mathbf{q}$. The tendency of the resolved scales is $\mathbf{q}_t^{\mathbf{R}}$, where all triadic interactions involve wavenumbers less than $T_R$. The remaining subgrid tendency $\mathbf{q}_t^{\mathbf{S}}$ has at least one wavenumber greater than $T_R$ which is involved in the triadic interactions. $\mathbf{q}_t^{\mathbf{S}}$ is further decomposed such that $\mathbf{q}_t^{\mathbf{S}}(t)=\overline{\mathbf{f}}+\widehat{\mathbf{q}}_t^{\mathbf{S}}(t)$, where $\overline{\mathbf{f}}\equiv\overline{\mathbf{q}_t^{\mathbf{S}}}$ is the time averaged subgrid tendency, and $\widehat{\mathbf{q}}_t^{\mathbf{S}}$ the fluctuating component. The values of $\overline{\mathbf{f}}$ are determined from the DNS, and $\widehat{\mathbf{q}}_t^{\mathbf{S}}$ is modelled as follows.

The $\widehat{\mathbf{q}}_t^{\mathbf{S}}$ is represented by the stochastic equation

$$\widehat{\mathbf{q}}_t^{\mathbf{S}}(t)=-\mathbf{D_d}\,\widehat{\mathbf{q}}(t)+\widehat{\mathbf{f}}(t)\,,\qquad(3)$$

where $\mathbf{D_d}$ is the subgrid drain dissipation matrix, $\widehat{\mathbf{q}}$ is the fluctuating component of $\mathbf{q}$, and $\widehat{\mathbf{f}}$ is a random forcing vector. As the present simulations have two vertical levels, $\mathbf{D_d}$ is a time independent $2\times2$ matrix, and $\widehat{\mathbf{f}}$ is a time dependent 2 element column vector. The $\mathbf{D_d}$ matrix is determined by post-multiplying both sides of (3) by $\widehat{\mathbf{q}}^\dagger(t_0)$, integrating over the turbulent decorrelation period $\tau$, ensemble averaging to remove the contribution of $\widehat{\mathbf{f}}$, and rearranging to produce

$$\mathbf{D_d}=-\left\langle\int_{t_0}^{t_0+\tau}\widehat{\mathbf{q}}_t^{\mathbf{S}}(\sigma)\widehat{\mathbf{q}}^\dagger(t_0)d\sigma\right\rangle\left\langle\int_{t_0}^{t_0+\tau}\widehat{\mathbf{q}}(\sigma)\widehat{\mathbf{q}}^\dagger(t_0)d\sigma\right\rangle^{-1},\quad(4)$$

where $\dagger$ denotes the Hermitian conjugate for vectors and matrices. The angled brackets denote ensemble averaging, with each ensemble member determined by shifting $t_0$ forward by one time step. The turbulence decorrelation time $\tau$, is chosen sufficiently large to capture the turbulent memory effects.

The model for $\widehat{\mathbf{f}}$ is determined by calculating the matrix $\mathcal{F}_{\mathbf{b}}=\mathbf{F_b}+\mathbf{F_b}^\dagger$, where $\mathbf{F_b}=\langle\widehat{\mathbf{f}}(t)\,\widehat{\mathbf{q}}^\dagger(t)\rangle$. Post-multiplying both sides of (3) by $\widehat{\mathbf{q}}^\dagger(t_0)$, and adding the conjugate transpose of (3) premultiplied by $\widehat{\mathbf{q}}(t_0)$ yields the Lyapunov equation

$$\left\langle\widehat{\mathbf{q}}_t^{\mathbf{S}}(t)\widehat{\mathbf{q}}^\dagger(t)\right\rangle+\left\langle\widehat{\mathbf{q}}(t)\widehat{\mathbf{q}}_t^{\mathbf{S}\dagger}(t)\right\rangle=$$
$$-\mathbf{D_d}\left\langle\widehat{\mathbf{q}}(t)\widehat{\mathbf{q}}^\dagger(t)\right\rangle-\left\langle\widehat{\mathbf{q}}(t)\widehat{\mathbf{q}}^\dagger(t)\right\rangle\mathbf{D_d}^\dagger+\mathcal{F}_{\mathbf{b}}\,.\quad(5)$$
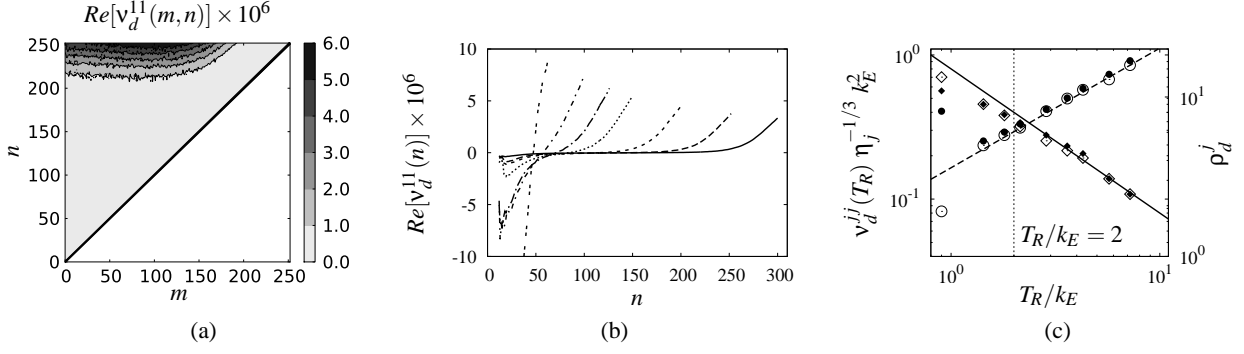
Figure 2: Drain eddy viscosity: (a) anisotropic coefficients $Re[D_d^{11}(m,n)]$ for $T_R = 252$; (b) isotropic coefficients $Re[D_d^{11}(n)]$ for $T_R = 63, 100, 126, 150, 200, 252, 300$; and (c) maximum values $v_{net}^{jj}(T_R)$ and power exponents $\rho_j$.

Given that $\mathbf{D_d}$ is known, $\mathcal{F}_b$ can now be calculated. At this point the formulation is general, and $\widehat{\mathbf{f}}$ is coloured noise. For the implementation of the stochastic subgrid parameterisation, however, it is sufficient to assume that $\widehat{\mathbf{f}}$ can be represented as the white noise process $\langle \widehat{\mathbf{f}}(t) \, \widehat{\mathbf{f}}^\dagger(t') \rangle = \mathcal{F}_b \, \delta(t-t')$.

The subgrid model in (3) represents the subgrid interactions in a stochastic manner. One can also do so deterministically, where the subgrid tendency is modelled according to $\widehat{\mathbf{q}}_t^{\mathbf{S}}(t) = -\mathbf{D_{net}} \, \widehat{\mathbf{q}}(t)$, with the net dissipation $\mathbf{D_{net}} = \mathbf{D_d} + \mathbf{D_b}$, and the backscatter dissipation $\mathbf{D_b} = -\mathbf{F_b} \langle \widehat{\mathbf{q}}(t) \, \widehat{\mathbf{q}}^\dagger(t) \rangle^{-1}$.

The equation governing the LES is the same as the DNS equation in (1), with $(q_t^S)_{mn}^j$ added to the right-hand-side, and solved over the wavenumber set $\mathbf{R}$ instead of $\mathbf{T}$. The most general form is the stochastic anisotropic representation

$$\left(q_t^S\right)_{mn}^j = -\sum_{l=1}^{2} D_d^{jl}(m,n)\widehat{q}_{mn}^l + \widehat{f}_{mn}^j + \bar{f}_{mn}^j . \quad (6)$$

In the anisotropic deterministic form, $D_d^{jl}(m,n)$ is replaced with $D_{net}^{jl}(m,n)$, and $\widehat{f}_{mn}^j$ is removed. In the isotropic parameterisations the matrices $\mathbf{D_d}$, $\mathcal{F}_b$ and $\mathbf{D_{net}}$ are isotropised. From this point onwards the subgrid coefficients are presented in eddy viscosity form, where the drain, backscatter and net eddy viscosities are related to their respective dissipations by $\mathbf{v_d} \equiv \mathbf{D_d}/[n(n+1)]$, $\mathbf{v_b} \equiv \mathbf{D_b}/[n(n+1)]$, and $\mathbf{v_{net}} \equiv \mathbf{D_{net}}/[n(n+1)]$.

**Subgrid eddy viscosities and scaling laws**

The DNS is truncated back to various values of $T_R$ to determine how the eddy viscosities change with resolution. We chose $\mathbf{v_0}$ to be consistent with it having been derived from a higher resolution DNS. Firstly we present the anisotropic $\mathbf{v_d}$ truncated back to $T_R = 252$, with $\tau = 288\Delta t = 2$ days. The real component of the upper diagonal $v_d^{11}(m,n)$ is illustrated in Fig. 2(a). At this resolution $v_d^{11}(m,n)$ increases with $n$, has only a weak dependence on $m$, and hence is approximately isotropic. The lower diagonal element $v_d^{22}(m,n)$ has a similar form, and the off-diagonal elements are small in comparison. These observations are also true for the backscatter and net eddy viscosities. We also find that $\mathbf{v_d} \approx \mathbf{v_{net}}/2 \approx -\mathbf{v_b}/2$. At lower truncation levels, however, the coefficients become more anisotropic, and the off-diagonal elements become proportionally more important.

Self similarity is most clearly illustrated by the isotropised profiles. The real component of the upper diagonal isotropised drain eddy viscosity $v_d^{11}(n)$ is illustrated in Fig. 2(b) for various truncation levels. It is clear that as the resolution increases the maximum value decreases, and the most negative value approaches zero. For truncations with $T_R > k_E$ the positive values of the eddy viscosities are concentrated in the last $k_E$ wavenumbers before truncation. This means that when plotted versus $n/T_R$ the profiles become steeper as resolution increases.

For the isotropised drain eddy viscosity, the change in magnitude ($v_d^{jj}(T_R)$) and slope ($\rho_d^j$) is quantified by least squares fitting the $v_d^{jj}(n)$ profiles to the function

$$v_d^{jj}(n) = v_d^{jj}(T_R) \, [n/T_R]^{\rho_d^j - 2} . \quad (7)$$

There are analogous expressions of (7) for $v_b^{jj}(n)$ and $v_{net}^{jj}(n)$. Note the form of $v_d^{jj}(n)$ prescribed in (7) is positive definite. The values of $v_d^{jj}(T_R)$ non-dimensionalised by $\eta_j^{-1/3} k_E^2$, are plotted as diamonds on the left vertical axis in Fig. 2(c) against $T_R/k_E$. The values of $\rho_d^j$ are plotted as circles on the right vertical axis in Fig. 2(c). The filled symbols represent $j = 1$, and the open symbols $j = 2$. There are two additional truncations plotted in in Fig. 2(c) made at $T_R = 400$ and 504, determined from a DNS with $T = 1008$. The data in Fig. 2(c) illustrates that as $T_R$ increases (more scales resolved), the strength, $v_d^{jj}(T_R)$, decreases and the steepness, $\rho_d^j$, increases.

The trend lines in Fig. 2(c) are fitted to data points for which $T_R/k_E > 2$, as this ensures that these data points have minimal subgrid interactions with the energy containing scales. The functional form of these trend lines are the eddy viscosity scaling laws and are explicitly outlined in [4]. Trend lines also exist for the eddy viscosities in baroclinic space. We can also determine the off-diagonal elements from these scaling laws as explicitly outlined in [4].

**Performance of LES with subgrid scale parameterisations**

We compare kinetic energy spectra at level 1 ($e_1$) of the DNS, to $e_1$ of various LES at two truncation levels $T_R = 126$ and 252. Observations made from the comparison of $e_1$ are consistent with comparisons of the level 2 spectra ($e_2$).

Firstly we test LESs with the raw anisotropic coefficients determined from the DNS. We compare both the stochastic and deterministic LES in Fig. 3(a), with each spectra offset for clarity. Whilst the stochastic parameterisation is the fundamental form [2], for the present flow configuration we find that the deterministic variant performs equally as well. The deterministic and stochastic parameterisations illustrate excellent agreement for both LES truncations $T_R = 126$ and 252.

Next we test the isotropic parameterisations using the raw coefficients. In Fig. 3(b) we compare the DNS to the stochastic and deterministic isotropic LES, both of which achieve excel-
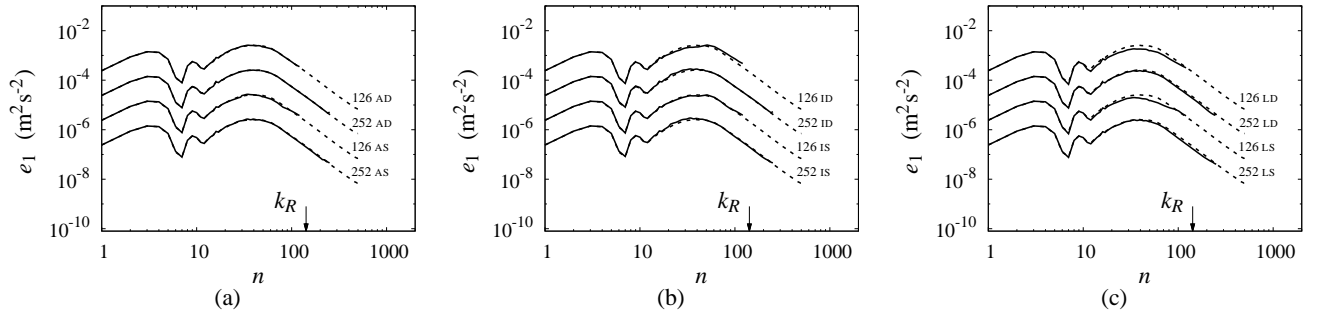
Figure 3: Spectra $e_1$ (DNS - dashed, LES - solid) using parameterisations: (a) anisotropic deterministic (AD), stochastic (AS); (b) isotropic deterministic (ID), stochastic (IS); (c) scaling laws deterministic (LD), stochastic (LS). Labelled with $T_R$ and parameterisation.

lent agreement at $T_R = 126$ and 252.

Finally we test LESs adopting isotropic subgrid parameterisations with coefficients defined by (7) and the scaling laws illustrated in Fig. 2(b). The spectra are compared in Fig. 3(c). Excellent agreement is achieved by both the deterministic and stochastic variants for truncations made at $T_R = 252$. At this resolution the baroclinic instability is explicitly resolved ($T_R > k_R$), and $v_d^{jj}(n)$ is positive definite (see Fig. 2(b)). By construction, the form representing these profiles in (7) can only be positive, which is adequate for $T_R = 252$. At the $T_R = 126$ truncation level, however, the baroclinic instability is not completely resolved ($T_R < k_R$), $v_d^{jj}(n)$ is in fact negative for certain $n$ (see Fig. 2(b)), and consequently the form in (7) does not represent these negative values. This is why the kinetic energy spectra is underestimated for both variants at $T_R = 126$. At this resolution some amount of negative eddy viscosity is required to further excite the LES in order to replicate the DNS spectra.

## Concluding remarks

Deterministic and stochastic subgrid parameterisations have been developed for oceanic flows representative of the ACC. The stochastic variant consists of a drain eddy viscosity, and a backscatter noise term. The deterministic version is governed solely by the net eddy viscosity, which represents the net effect of the drain and backscatter. These wavenumber dependent eddy viscosity matrices have been derived self-consistently from the statistics of higher resolution DNS.

We have undertaken various LESs with subgrid coefficients determined from the DNS. The anisotropic deterministic and stochastic parameterisations reproduce the DNS spectra at $T_R = 126$ and 252. Both the deterministic and stochastic isotropic parameterisations using raw coefficients also reproduce the spectra within the inertial range. Isotropic variants with coefficients determined by the scaling laws also adequately reproduce the kinetic energy spectra of the DNS.

To further improve the applicability of these scaling laws, current research is investigating how they may change with Rossby radius. In the future we also hope to further verify these scaling laws by applying the present subgrid modelling approach to more complex mutli-level primitive equation models incorporating more complete dynamics and physics.

## Acknowledgements

## References

[1] Frederiksen, J. S., Precursors to blocking anomalies: the tangent linear and inverse problems, *J. Atmos. Sci.*, **55**, 1998, 2419–2436.

[2] Frederiksen, J. S. and Davies, A. G., Eddy viscosity and stochastic backscatter parameterizations on the sphere for atmospheric circulation models, *J. Atmos. Sci*, **54**, 1997, 2475–2492.

[3] Frederiksen, J. S. and Kepert, S. M., Dynamical subgrid-scale parameterizations from Direct Numerical Simulations, *J. Atmos. Sci.*, **63**, 2006, 3006–3019.

[4] Kitsios, V., Frederiksen, J. S. and Zidikheri, M. J., Scaling laws for parameterisations of subgrid eddy-eddy interactions in simulations of oceanic circulations, *to be submitted*, **ftp.csiro.au/Kitsios/Kitsios2012.pdf**.

[5] Kitsios, V., Frederiksen, J. S. and Zidikheri, M. J., Subgrid model with scaling laws for atmospheric simulations, *J. Atmos. Sci.*, **69**, 2012, 1427–1445.

[6] Leith, C. E., Atmospheric predictability and two-dimensional turbulence, *J. Atmos. Sci.*, **28**, 1971, 145–161.

[7] Manabe, S., Hahn, D. G. and Holloway, J. L., Climate simulations with GFDL spectral models of the atmosphere: effects of spectral truncation, *GARP Pub. Ser.*, **22**, 1979, 41–94.

[8] Phillips, H. and Rintoul, S., A mean synoptic view of the subantarctic front south of australia, *J. Phys. Oceanogr.*, **32**, 2002, 1536–1553.

[9] Smagorinsky, J., General circulation experiments with the primitive equations: I. the basic experiment, *Mon. Wea. Rev.*, **91**, 1963, 99–164.

[10] Zidikheri, M. J. and Frederiksen, J. S., Stochastic subgrid parameterizations for simulations of atmospheric baroclinic flows, *J. Atmos. Sci.*, **66**, 2009, 2844–2858.

[11] Zidikheri, M. J. and Frederiksen, J. S., Stochastic modelling of unresolved eddy fluxes, *Geophysical and Astrophysical Fluid Dynamics*, **104**, 2010, 323–348.